SIMULATION AND EXPERIMENTAL VALIDATION OF A356 AND AZ91 ALLOY FLUIDITY IN A GRAPHITE MOLD

V. E. Bazhenov [iD], A. V. Petrova, A. A. Rizhsky, Yu. V. Tselovalnik, A. V. Sannikov, and V. D. Belov
Foundry Department, National University of Science and Technology (MISiS), Leninskiy pr. 4, Moscow, Russia 119049

Abstract

Graphite mold casting is a promising technique owing to its ability to provide high cooling rates and suitability for many types of alloys. The fluidity of A356 aluminum and AZ91 magnesium alloys cast into graphite molds was determined at casting temperatures of 670 °C–810 °C. As expected, the fluidity of AZ91 was lower than that of A356. The critical solid fractions for A356 aluminum and AZ91 magnesium alloys were determined by comparing simulated spiral fluidity test lengths with those obtained experimentally. For graphite mold casting, the critical solid fractions for A356 and AZ91 alloys were in the range of 0.12–0.15 and 0.13–0.17, respectively.

Keywords: *fluidity simulation, graphite mold, critical solid fraction, spiral test, A356 alloy, AZ91 alloy*

Introduction

Graphite mold casting is a promising technique owing to its ability to provide an alloy cooling rate that is nearly twice as high as that of the conventional steel mold gravity casting.[1,2] Many types of alloys can be cast using graphite molds,[3–10] and graphite is a solid lubricant, thus eliminating the need for die coatings and other lubricants.[10] The machinability of graphite is also known to be higher than that of steel[11]; most commonly, graphite molds are made using CNC milling of graphite blocks.

Due to the high cooling rate, there is a substantial risk of misrun defect formation during graphite mold casting. It is known that the alloy fluidity is responsible for misrun formation during casting. In this study, two alloys were selected for graphite mold fluidity testing: A356 aluminum alloy, which has the most common high-fluidity casting alloy, and AZ91 magnesium alloy, which has lower fluidity than A356.[12]

Ensuring adequate predictability of fluidity and misruns during casting simulation is substantially challenging.[13] To align the actual casting process with the simulation results, the thermal properties of the materials, such as the interfacial heat-transfer coefficient (IHTC) at the mold/casting interface and the critical solid fraction, are required. The critical solid fraction is the point at which the melt flow in the mold channel stops.[14–16] Previously, IHTCs were determined for A356/graphite and AZ81/graphite alloy/-mold combinations,[1] which can be utilized in this work. The previous literature shows that a spiral fluidity test can be applied to determine the critical solid fraction and IHTC. When the correct value of the critical solid fraction is established during the simulation, the simulated spiral length must be equal to the experimental spiral test length.[17–19]

The objective of this study was to determine the critical solid fractions applicable to the graphite mold gravity casting of A356 aluminum and AZ91 magnesium alloys using spiral tests by comparing simulated spiral lengths with those obtained experimentally.

Materials and Methods

A356 and AZ91 melts were prepared in a 20-kHz induction furnace; the charges of the melts were 4 kg and 2.5 kg for A356 and AZ91, respectively. Commercial A356 aluminum alloy ingots were melted using a clay graphite crucible. Prior to casting, the A356 melt was treated with refining flux and degassed with hexachloroethane. The

duration of each treatment was almost 3 min; after degassing, the melt was held for 15 min before casting.

Commercial purity metals were used to prepare the AZ91 alloy, the melting of which was performed in a steel crucible under a carnallite ($MgCl_2 \cdot KCl$) flux. The AZ91 melt was treated with carnallite flux for 3 min and held for 15 min before casting.

The A356 alloy composition was determined using a Bruker Q4 TASMAN optical emission spectrometer. The AZ91 magnesium alloy composition was determined using a Tescan Vega SBH3 scanning electron microscope, which was equipped with an Oxford energy dispersive spectroscopy analysis system. Alloy compositions are given in Table 1.

The spiral fluidity test applied to determine alloy fluidity was designed by the authors and is shown in Figure 1. A mold with a spiral cavity was produced from high-density low-ash graphite GMZ grade (Russia) blocks using CNC milling. The fluidity test had a channel with a constant cross-sectional area of 15×15 mm^2. The melt was poured into a cup made from sand with a furan binder. Before filling, a timber stopper and a K-type thermocouple were installed in the cup. When the melt had been poured and had become calm, the stopper was removed from the cup, and the casting temperature was measured using the thermocouple. For each alloy, the fluidity was determined approximately 10 times at various casting temperatures. After the first idle pouring, the mold was heated to almost 80 °C, and between fluidity test casting trials, the mold temperature was measured using the thermocouple, which was placed between the lower and upper parts of the mold. The measured temperature was in the range of 60–100 °C.

Various commercial simulation softwares are available for modeling of casting processes.[20] We used ProCast 2018 to simulate graphite mold spiral test filling. ProCast uses the finite element method to perform Fourier heat conduction and Navier–Stokes calculations.[21] Calculation details and equations can be found elsewhere.[22–24]

First, the spiral test filling was simulated with the stopper installed in the pouring cup in order to identify the moment at which the melt temperature in the pouring cup was equal to the casting temperature. Next, a simulation was performed in which the stopper was removed at the aforementioned moment. An interpenetrating mesh algorithm was employed to generate a realistic simulation of stopper removal. The thermal properties and IHTC of the materials used for the simulation are shown in Figures 2 and 3, respectively.[25–28] The thermal properties of the alloys for actual compositions were calculated using the CompuTherm LLC thermodynamic database in ProCast, and a constant graphite density was set as 1.78 g/cm^3.[25] The timber thermal conductivity, heat capacity, and density were 0.16 W/mK, 1.63 J/gK, and 0.68 g/cm^3, respectively.[29] The IHTC for the alloy/timber pairing was unknown; however, this was not relevant for our simulation. When the cup was filled with the alloy, it cooled mainly when in contact with the sand mold due to the very low thermal conductivity and density of the timber compared with sand. In this regard, we installed an alloy/timber IHTC as 500 W/m^{2}K, which is lower than an alloy/sand mold IHTC.

Results and Discussion

Figure 3 presents the IHTC versus the casting surface temperature for A356/graphite and AZ91/graphite couples. In the source article,[1] when the casting surface temperature transitions from the casting temperature to the alloy liquidus temperature, the IHTC increases from 100 to 4700 W/m^{2}K. It takes a few seconds to correctly measure the temperature due to thermocouple hot-end heating. Because of this, the measured temperature is incorrect until the response time has passed. The mentioned parts of the IHTC versus temperature curves are also incorrect. A constant IHTC of 4700 W/m^{2}K is assumed in between pouring and the alloy's liquidus temperature.

The experimental spiral lengths for the A356 and AZ91 alloys cast into graphite molds at various temperatures are shown in Figure 4. The casting temperatures vary from 670 °C to 810 °C. The experimental spiral length values are given in the form of linear dependences. To calculate the confidential limits, the results obtained at close casting temperatures were grouped, and for each group, the standard deviation and confidence limit were calculated using a standard method. The two groups in the range of 670 °C–700 °C and 740 °C–810 °C were used for the A356 alloy. For the AZ91 alloy, three groups were identified: 670 °C–680 °C, 720 °C–740 °C, and 770 °C–810 °C.

For the A356 alloy cast in graphite molds at 670 °C and 810 °C, the spiral lengths were 598 and 890 mm, respectively. This means that an increase in the casting temperature of 140 °C generates a one-third increase in the spiral length. As expected, the AZ91 magnesium alloy spiral lengths were lower. When the AZ91 alloy was cast in graphite molds at 670 °C and 810 °C, the spiral lengths

Table 1. Alloy Compositions

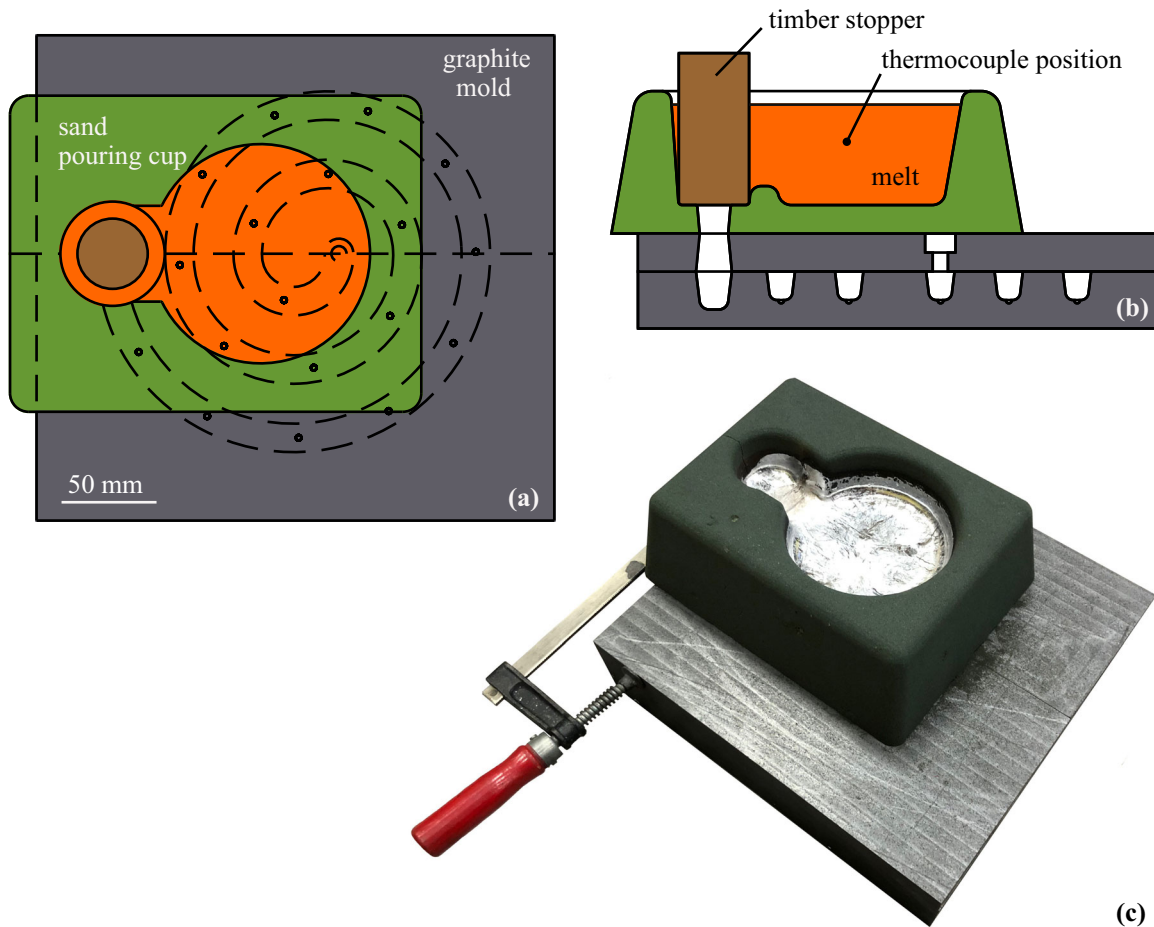| Alloy	Alloying elements content (wt%)				
	Al	Mg	Si	Zn	Mn
A356	Bal.	0.27	7.45	–	–
AZ91	9.18	Bal.	–	0.76	0.46

Figure 1. Graphite mold used for spiral fluidity test: (a) top view; (b) cross section; and (c) mold after pouring.

were 441 and 645 mm, respectively. Increasing the AZ91 alloy casting temperature by 140 °C also resulted in a one-third increase in the spiral length. Figure 3 shows that the IHTC versus casting surface temperature relationship is similar for both the A356 and AZ81 alloys. The heat of fusion of the A356 alloy and that of the AZ91 alloy is also similar (389 and 373 J/g, respectively).[30] However, their room temperature densities are 2.69 and 1.81 g/cm^3, respectively.[30] This means that the latent heat released during the solidification of 1 cm^3 of A356 and AZ91 alloy is 1046 and 674 J, respectively. Therefore, the difference between the alloy fluidity of the two materials occurs mostly due to differences in heat released during alloy solidification.

In Figure 5, the experimental spiral test data are compared with simulated misrun prediction patterns for A356 alloy casting at 780 °C. The critical solid fraction at which the melt flow stops is set to 0.12. The area in the melt flow simulation where the solid fraction reaches the critical solid fraction (0.12) is colored orange (see legend in Figure 5). In a real casting process, the melt flow is impeded and stopped when the critical solid fraction is reached. However, in the simulation results, we can see only the areas

where the solid fraction reaches the critical value. In fact, during the simulation process, the melt flow continues when the critical solid fraction is reached. As can be seen from the simulated spiral top view (Figure 5c), the area where the critical solid fraction is reached (blue line) corresponds with the area in which misruns start to form during real spiral casting (blue line in Figure 5a). This is not useful for spiral length prediction because the spiral end (the area where the melt flow stops) cannot be identified in the simulated spiral top view. Figure 5b and d present the bottom view of the experimental spiral and simulated misrun layout, respectively. In the simulated misrun prediction results, the areas where the critical solid fraction is reached alternate with the areas where the solid fraction is less than critical. It is assumed that in simulation results, the spiral ends where the areas with a solid fraction are lower and higher than critical are equal. This proposed spiral end is indicated by the red line in Figure 5d. The aforementioned assumption is used in A356 and AZ91 alloy simulation analysis at various casting temperatures and critical solid fractions.

The experimental and simulated spiral lengths for various A356 alloy critical solid fractions are shown in Figure 6;
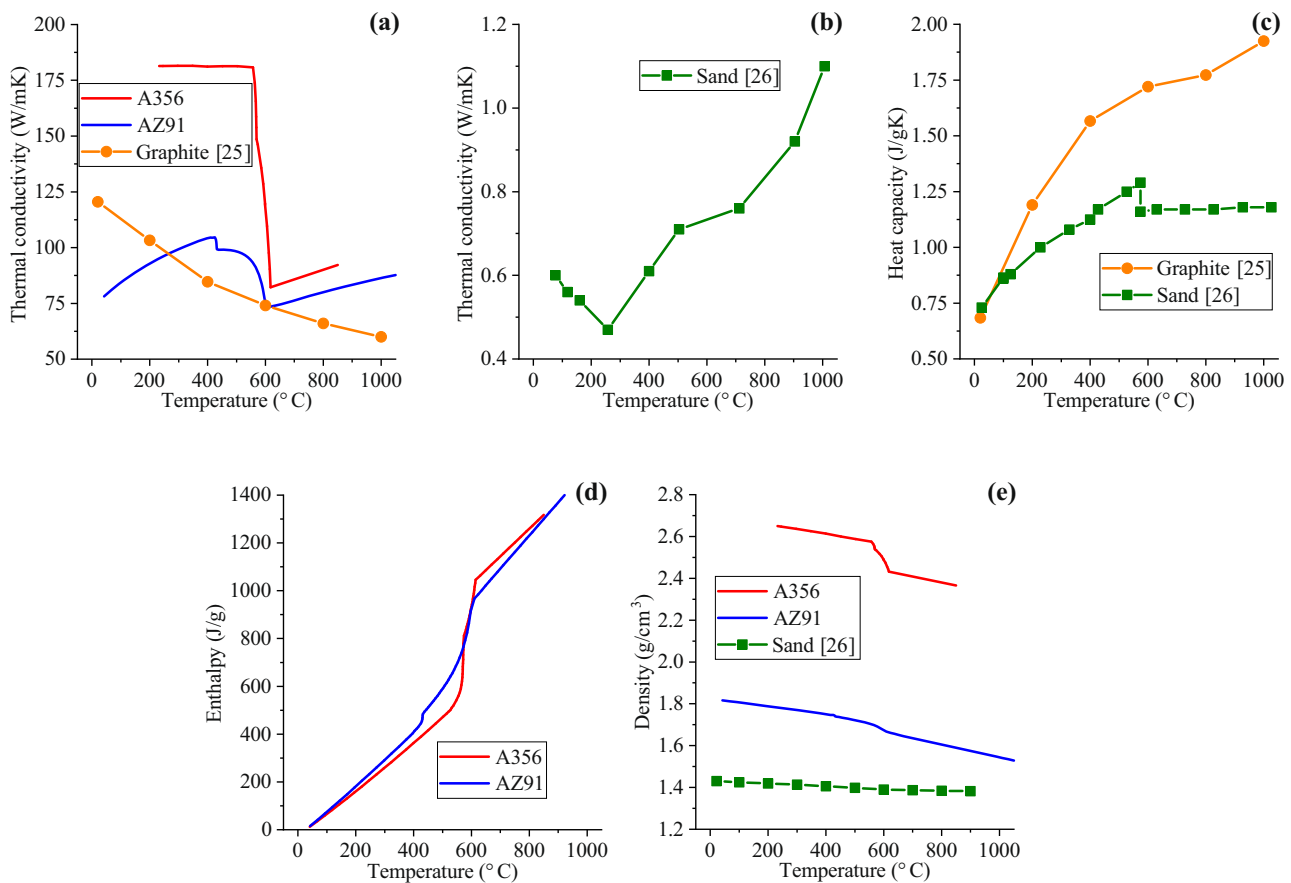
Figure 2. Thermal properties: (a, b) thermal conductivity; (c) heat capacity; (d) enthalpy; and (e) density of the materials used for simulation.
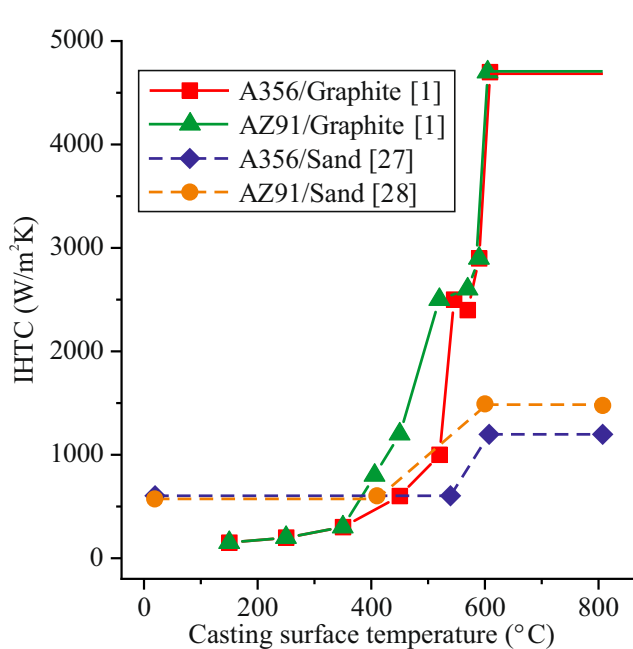

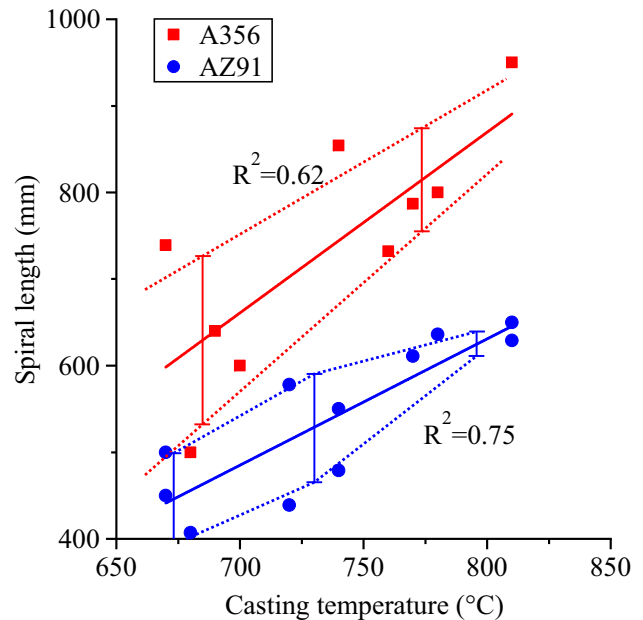Figure 3. IHTC versus casting surface temperature for A356/graphite and AZ91/graphite alloy/mold couples.

Figure 4. Experimental spiral length versus casting temperature for A356 and AZ91 alloys cast into graphite molds.
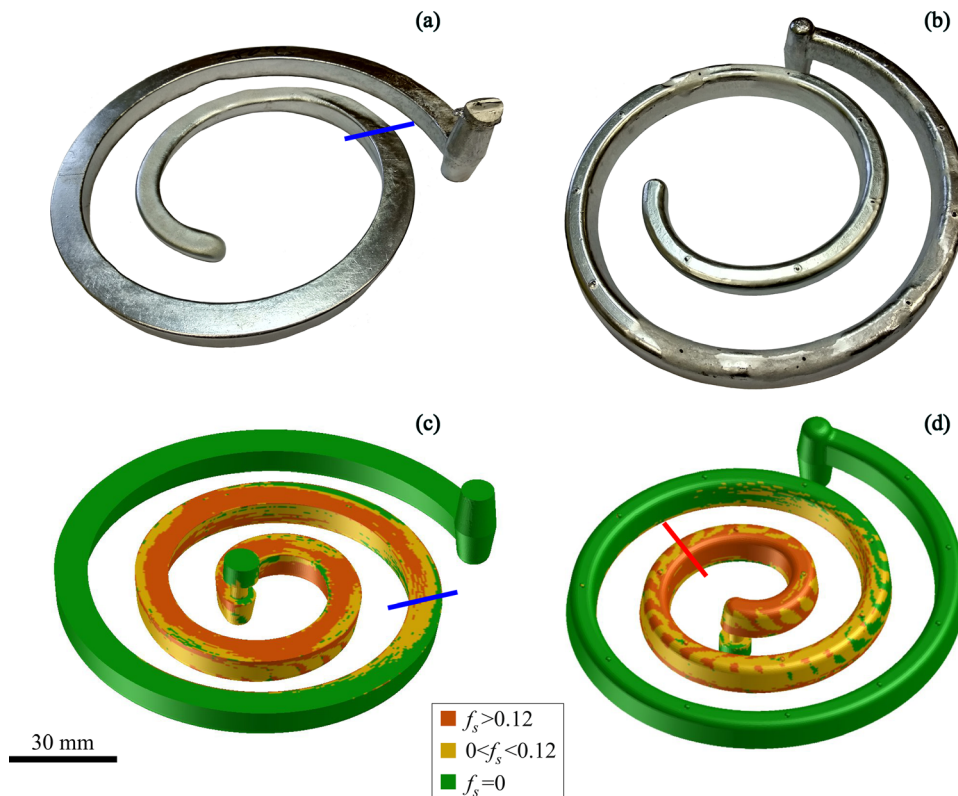
Figure 5. Experimental spiral test of A356 alloy cast at 780 °C: (a) top view and (b) bottom view. Misrun prediction simulation results for the same alloy and casting conditions at a critical solid fraction of 0.12: (c) top view and (d) bottom view.
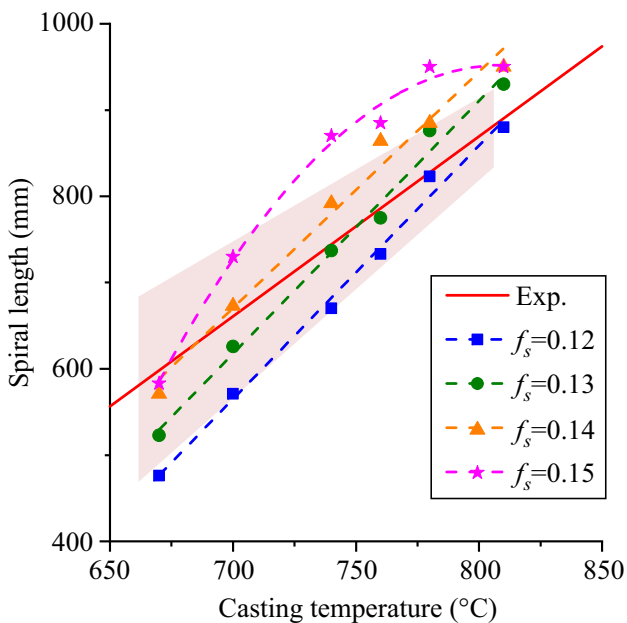

Figure 6. Experimental and simulated spiral lengths for A356 alloy cast into a graphite mold at various critical solid fractions.

the confidence limit for experimental results is indicated as the filled area. As for the simulation results, the spiral lengths were calculated for different critical solid fractions, but the graph presented the results for critical solid fractions from 0.12 to 0.15. The simulated and experimental spiral lengths diverge at critical solid fractions of < 0.12 and > 0.15. A change in the critical solid fraction of 0.03 is significant and leads to a change in the simulated spiral length by almost 100 mm. At a casting temperature of 670 °C, the best fit between the experimental and simulated spiral lengths is obtained at a critical solid fraction of 0.15. If the casting temperature is higher (810 °C), the simulated and experimental spiral lengths have the best fit at a critical solid fraction of 0.12.

In Figure 7, the experimental and simulated AZ91 alloy spiral lengths are compared at various critical solid fractions (the filled area on the figure indicates the confidence limit for experimental results). The experimental and simulated spiral lengths are similar at a critical solid fraction range of 0.13–0.17. At a low critical solid fraction (0.13), the experimental and simulated spiral lengths match at high casting temperatures (810 °C). At a casting temperature of 670 °C, the experimental and simulated spiral lengths match at a higher critical solid fraction (0.17).

These results show that the casting temperature effects the critical solid fraction. For both A356 aluminum and AZ91 magnesium alloys, the critical solid fraction is higher at lower casting temperatures. High confidence limits for
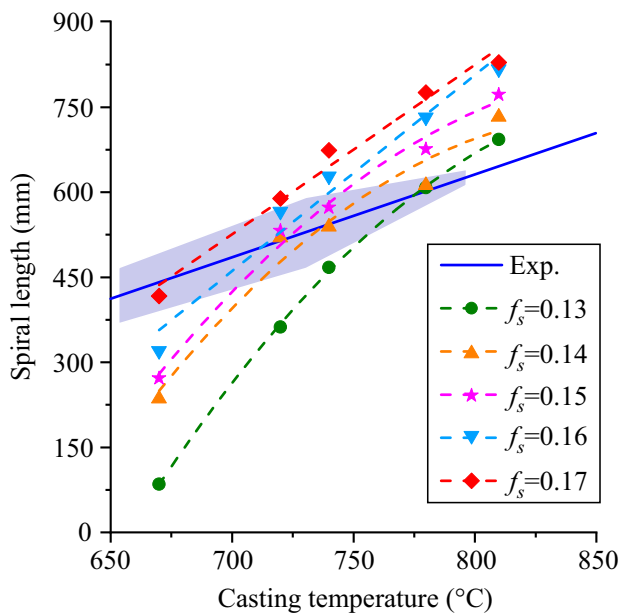
Figure 7. Experimental and simulated spiral lengths for AZ91 alloy cast into a graphite mold at various critical solid fractions.

experimental spiral length (up to ± 100 mm for the A356 alloy and up to ± 60 for the AZ91 alloy) were observed. These fluidity test results are insufficient to support highly reliable statements; therefore, further experiments are required. Based on the results obtained, we can conclude that for the A356 aluminum alloy, the critical solid fraction was in the range of 0.12–0.15. For the AZ91 alloy, the critical solid fraction was in the range of 0.13–0.17.

It is known that the critical solid fraction is related to the coherency point.[31] The coherency point is the fraction of the solid phase at which a continuous, three-dimensional dendritic network is developed in a partially solidified melt.[31,32] This means that the melt flow is hindered substantially after dendritic network formation. In line with our experimental results, an increase in the cooling rate leads to a decrease in the coherency point of the A356 aluminum alloy.[33] This is because the growth rate of the dendrite arm tip increases with an increase in the cooling rate; therefore, the dendritic network forms at a lower solid fraction when a high cooling rate is used.[34] The result is the opposite for the AZ91 alloy; increasing the cooling rate increases the coherency point.[35] In other work, the relationship between these two parameters is more complex.[36] These ambiguous results mean that the effect of the cooling rate on the coherency point of the alloy and the critical solid fraction are unclear.

Conclusions

The fluidity test spiral lengths for the casting of the A356 alloy into a graphite mold at temperatures of 670 °C and

810 °C were 598 and 890 mm, respectively. As expected, the fluidity of the AZ91 magnesium alloy was lower under the same casting conditions. Spiral lengths of 441 and 645 mm were measured at temperatures of 670 °C and 810 °C, respectively. For both alloys, the change in the casting temperature by 140 °C leads to a one-third increase in the spiral length. The differences between the A356 and AZ91 alloy fluidities are associated with the differences in the heat released during the solidification of a given volume of each alloy.

The critical solid fractions for A356 aluminum and AZ91 magnesium alloy graphite mold gravity casting were determined applying spiral fluidity test. For the A356 aluminum alloy, the critical solid fraction was 0.12–0.15. Similar critical solid fraction values were obtained for the AZ91 alloy (0.13–0.17).

REFERENCES

1. V.E. Bazhenov, Yu.V. Tselovalnik, A.V. Koltygin, V.D. Belov, Submitted to Int. J. Metalcast.
2. J. Major, M. Hartlieb, Int. J. Metalcast. **3**, 43 (2009)
3. S. O'Connor, Adv. Mater. Process. **166**, 29 (2008)
4. S. O'Connor, AMMTIAC Quart. **2**, 3 (2007)
5. L. Jia, D. Xu, M. Li, J. Guo, H. Fu, Met. Mater. Int. **18**, 55 (2012)
6. V. Zanchuk, Adv. Mater. Process. **162**, 66 (2004)
7. V. Zanchuk, Die Cast Eng. **1**, 38 (2006)
8. L. Wang, H. Yan, J. Teng, X. Liu, X. Wang, Y. Su, J. Guo, J. Mater. Res. Tech. (in press). https://doi.org/10.1016/j.jmrt.2020.02.071. (2020)
9. G. Baumeister, D. Buqezi-Ahmeti, J. Glaser, H.-J. Ritzhaupt-Kleissl, Microsyst. Technol. **17**, 289 (2011)
10. W.C. Chen, F.Y. Teng, C.C. Hung, Mater. Sci. Eng. C **35**, 231 (2014)
11. A.Y.C. Nee, *Handbook of Manufacturing Engineering and Technology* (Springer, London, 2015)
12. H. Huang, Y.X. Wang, P.H. Fu, L.M. Peng, H.Y. Jiang, W.Y. Xu, Int. J. Cast Met. Res. **26**, 213 (2013)
13. M. Sabatino, L. Arnberg, D. Apelian, Int. J. Metalcast. **2**, 17 (2008)
14. T.O. Mbuya, Trans. Am. Foundry. Soc. **114**, 163 (2006)
15. M. Di Sabatino, L. Arnberg, Metall. Sci. Technol. **22**, 9 (2004)
16. K.R. Ravi, R.M. Pillai, K.R. Amaranathan, B.C. Pai, M. Chakraborty, J. Alloys Compd. **456**, 201 (2008)

17. Y. Motoyama, H. Tokunaga, M. Yoshida, T. Maruyama, T. Okane, J. Mater. Process. Tech. **276**, 116394 (2020)

18. J. Jakumeit, E. Subasic, M. Bünck, *Shape Casting: 5th International Symposium 2014* (Wiley, San Diego, 2014), pp. 253–260

19. V.E. Bazhenov, A.V. Petrova, A.V. Koltygin, Int. J. Metalcast. **12**, 514 (2018)

20. M.A.A. Khan, A.K. Sheikh, Int. J. Simul. Model. **17**, 197 (2018)

21. ESI Group, ProCAST 2010.0 User's Manual (ESI Group, 2010), https://myesi.esi-group.com/system/files/documentation/ProCAST/2010/ProCAST_20100_UM.pdf. Accessed 1 August 2019

22. L. Yang, L.H. Chai, Y.F. Liang, Y.W. Zhang, C.L. Bao, S.B. Liu, J.P. Lin, Intermetallics **66**, 149 (2015)

23. S.-L. Lu, F.-R. Xiao, Z.-H. Guo, L.-J. Wang, H.-Y. Li, B. Liao, Appl. Therm. Eng. **93**, 518 (2016)

24. J.A. Dantzig, M. Rappaz, *Solidification* (EPFL Press, Lausanne, 2009), pp. 105–151

25. E.I. Zhmurikov, I.V. Savchenko, S.V. Stankus, O.S. Yatsuk, L.B. Tecchio, Nucl. Instrum. Methods Phys. Res. Sect. A **674**, 79 (2012)

26. G. Palumbo, V. Piglionico, A. Piccininni, P. Guglielmi, D. Sorgente, L. Tricarico, Appl. Therm. Eng. **78**, 682 (2015)

27. V.E. Bazhenov, A.V. Koltygin, Yu.V. Tselovalnik, Russ. J. Non-Ferr. Met. **57**, 686 (2016)

28. V.E. Bazhenov, A.V. Petrova, A.V. Koltygin, Yu.V. Tselonalnik, Tsvetnye Metally **2017**, 89 (2017)

29. W.P. Goss, R.G. Miller, *Proceedings of Thermal Performance of the Exterior Envelopes of Buildings* (ASHRAE, New York, 1992), pp. 193–203

30. A.S.M. Handbook, *Properties and selection: Nonferrous alloys and special-purpose materials*, vol. 2, 10th edn. (ASM International, Materials Park, 2002), pp. 624–1546

31. A.K. Dahle, P.A. Tøndel, C.J. Paradies, L. Arnberg, Metall. Mater. Trans. A **27**, 2305 (1996)

32. A.K. Dahle, L. Arnberg, Acta Mater. **45**, 547 (1997)

33. N.L.M. Veldman, A.K. Dahle, D.H. StJohn, L. Arnberg, Metall. Mater. Trans. A **32**, 147 (2001)

34. L. Arnberg, G. Chai, L. Backerud, Mater. Sci. Eng., A **173**, 101 (1993)

35. M. Król, T. Tański, G. Matula, P. Snopiński, A. Tomiczek, Arch. Metall. Mater. **60**, 2993 (2015)

36. F. Yavari, S.G. Shabestari, Int. J. Cast Met. Res. **32**, 85 (2019)